POLITECNICO DI TORINO
Repository ISTITUZIONALE

Enhancing properties and water resistance of PEO-based electrospun nanofibrous membranes by photo-crosslinking

Original
Enhancing properties and water resistance of PEO-based electrospun nanofibrous membranes by photo-crosslinking / Kianfar, P., Vitale, A., Dalle Vacche, S., Bongiovanni, R.. - In: JOURNAL OF MATERIALS SCIENCE. - ISSN 0022-2461. - ELETTRONICO. - 56:(2021), pp. 1879-1896. [10.1007/s10853-020-05346-3]

Availability:
This version is available at: 11583/2847508 since: 2022-06-02T11:28:40Z

Publisher:
Springer - Handling Editor: Gregory Rutledge

Published
DOI:10.1007/s10853-020-05346-3

Terms of use:

This article is made available under terms and conditions as specified in the corresponding bibliographic description in the repository

Publisher copyright

(Article begins on next page)

30 June 2026

J Mater Sci

Polymers & biopolymers

Enhancing properties and water resistance of PEO-based electrospun nanofibrous membranes by photo-crosslinking

Parnian Kianfar[1,*], Alessandra Vitale[1,*], Sara Dalle Vacche[1], and Roberta Bongiovanni[1]

[1] *Department of Applied Science and Technology, Politecnico Di Torino, Corso Duca degli Abruzzi 24, 10129 Torino, Italy*

Received: 17 May 2020
Accepted: 12 September 2020

© The Author(s) 2020

ABSTRACT

In this study, modified fibrous mats of poly(ethylene oxide) (PEO) were fabricated through the versatile technique of electrospinning. Acrylic monomers were added to PEO with different composition ratios, and the mats were irradiated. The kinetics of photo-cross-linking reaction in the presence of the acrylic cross-linkers, as well as the structural, thermal and mechanical properties of the nanofibers, were studied. The morphology of the fibrous membranes before and after water treatment was monitored, and the insoluble fraction of the fibers was measured. As a result, by tuning the photo-cross-linking reaction, the control over fibers properties was feasible. The photo-cured PEO-based nanofibrous mats showed the solubility resistance needed to use them as membranes and to apply them in aqueous environments, as in water treatment processes and biomedical applications.

Handling Editor: Gregory Rutledge.

Parnian Kianfar and Alessandra Vitale contributed equally to the work

Address correspondence to E-mail: parnian.kianfar@polito.it; alessandra.vitale@polito.it

https://doi.org/10.1007/s10853-020-05346-3

Published online: 01 October 2020

GRAPHICAL ABSTRACT

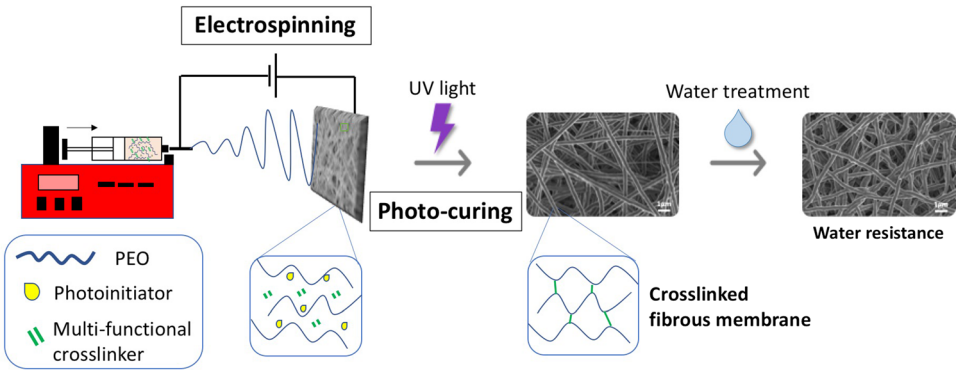

Introduction

Electrospinning is a unique technique to produce fine polymer fibers through electrostatic process [1, 2] and obtain mats that can be used as membranes. Nanofibrous electrospun membranes are attracting tremendous attention in numerous applications, such as tissue engineering, drug delivery, insulating materials, food encapsulation, energy conversion, filtration, sensing systems and protective clothing [3–11], especially thanks to their high surface area-to-volume ratio, large surface functionality and excellent mechanical performances. One of the main advantages of electrospinning is surely related to the possibility of processing a large set of polymers, both natural and synthetic [12–15]. The affecting parameters in the transformation of polymer solutions or melt into nanofibers are associated with solution properties, processing variables and environment conditions. For instance, the polymer solution should provide an optimum amount of viscosity, conductivity and surface tension [16–19].

Polyethylene oxide (PEO) is a crystalline, thermoplastic polymer with general formula of $(–O–CH_2–CH_2–)_n$. Unlike many other polymer systems, PEO is commercially available in a wide range of molecular weights from tens of repeating units (in this case the polymer is called polyethylene glycol, PEG) to higher than a million [20]. PEO is colorless, odorless, stable against heat and hydrolysis, acts as inert substance to many chemical reagents and is a non-toxic polymer. Its biocompatibility, non-immunogenicity, alongside interesting physicochemical properties, make PEO an excellent candidate for biomedical applications, particularly as scaffolds in tissue engineering [21, 22] and biocompatible coatings [23–25], together with other wide application fields, such as filtration for CO_2 separations [26–28] and energy storage applications [29, 30]. However, this polymer is soluble in water as well as in organic solvents, and as a result, its application domains are limited [21].

Over recent decades, several methods have been reported to tackle this obstacle of solubility. First of all, cross-linking (i.e., the formation of a polymer network) can hinder the solubility or even make the polymer insoluble. Consequently, cross-linked PEO introduces new applications in the above-mentioned fields such as surgical dressings [3, 31], drug delivery systems [9], filtration and membranes with controlled permeability [32]. Cross-linking techniques can be categorized in the following three subgroups: (i) cross-linking by gamma irradiation [33], which was introduced as an efficient method for cross-linking dilute aqueous PEO solutions, while in solid state or bulk such method demands a very high radiation dosage [34]; (ii) cross-linking by UV irradiation [35, 36], which is an accessible and eco-friendly technique applicable to PEO both in solid form and in solution [37]; and (iii) chemical cross-linking [38] by the introduction of reactive end-groups in the polymer structure or by using low molecular weight cross-linkers [39].

PEO in the field of electrospinning mainly acts as a carrier/template for non-electrospinnable or hardly electrospinnable polymers, such as chitosan [13, 40], alginate [41, 42], collagen [43], hyaluronic acid [44] and keratin [45]. In these studies, a cross-linking reaction (upon UV irradiation, thermal treatment, chemical treatment, vapor deposition, etc.) is performed with the aim of enhancing the properties of the blend electrospun membranes. However, in many of these works, PEO is extracted from the electrospun membrane [41, 44], leaving only the main component of the fibers.

UV-induced cross-linking is an interesting method for the modification of polymeric membranes in order to increase their mechanical strength, solvent resistance or permeability. Among the curing processes, the use of light to induce cross-linking reactions has several advantages, such as short conversion times, low energy consumption, ambient temperature operations and selective curing with an intimate control both in time and space. One drawback in UV cross-linking is the light penetration power, which is limited to a layer of around 200 μm from the surface [46]. But this obstacle does not apply to thin electrospun membranes.

Upon UV irradiation, preferably in the presence of a suitable photo-initiator, hydrogens of the PEO carbon chain can be abstracted and radicals generated; the combination of these polymeric radicals yields a cross-linked network [39]. PEO can also undergo chain scission during UV irradiation: C–O bonds can break resulting in a pair of free radicals. Generally, the probability of cross-linking in aqueous medium is higher, whereas in bulk chain scission predominates over cross-linking [20, 36, 37]. However, the competition between the two reactions greatly depends on irradiation time, photo-initiator concentration and oxygen presence. Additionally, the introduction of a cross-linking agent accelerates the photo-induced reaction among PEO chains, limiting their degradation [9, 37, 47].

The cross-linking of PEO electrospun membranes has not been extensively studied. In fact, few works [48] [49] investigating the UV-cross-linking of PEO electrospun membranes by using an acrylic cross-linker (i.e., pentaerythritol triacrylate) are present in the literature, but although the reaction was demonstrated to be successful, the cross-linking efficiency and the fibrous morphology stability of the mats were not discussed. In a recent work, Şimşek et al. [50] proposed such PEO-based electrospun membrane as a biomedical coating for metallic implants; after immersion in distilled water of the PEO electrospun-coated Ti implant, a fused fibers morphology was reported.

Herein, two multifunctional acrylic monomers, namely polyethylene glycol diacrylate (PEGDA) and trimethylol propane triacrylate (TMPTA), were used as cross-linking agents for PEO fibers [51]. PEGDA is non-toxic, biodegradable and provokes minimal immune system response, and thus is an excellent candidate for PEO cross-linking [51]. TMPTA, as a trifunctional cross-linker, has been widely used in hydrogels synthesis with further application in biomedical, pharmaceutical and environmental fields [52, 53].

In this work, photo-cross-linking of PEO electrospun nanofibrous mats containing a cross-linker was applied to enhance the membrane properties and in particular to overcome the PEO solubility issues. PEO-based fibers were produced by electrospinning of aqueous polymer solutions containing benzophenone as photo-initiator and different contents of a multifunctional cross-linking agent (i.e., PEGDA or TMPTA); for PEGDA and TMPTA, similar PEO/acrylate group (mol/mol) ratios were used. The electrospun fibrous membranes were then photo-cured. The effect of the type and amount of cross-linker on the photo-curing reaction and on the final properties of the nanofibrous membranes was evaluated. Accordingly, the photo-cross-linking reaction kinetics and its efficiency were monitored through photo-differential scanning calorimetry (photo-DSC), Fourier transform Infrared (FTIR) spectroscopy and insoluble fraction measurements. The final morphology, porosity, thermal and mechanical properties, permeability and water resistance of the photo-cross-linked membranes were studied.

Experimental

Materials

High molecular weight polyethylene oxide (MW 1,000,000 g/mol), benzophenone (≥ 99%), polyethylene glycol diacrylate (MW 575 g/mol, viscosity 57 cP) and trimethylolpropane triacrylate (MW 296 g/mol, viscosity 70–12 cP) were purchased from Sigma-Aldrich.

Sample preparation

5 wt% aqueous solution of PEO was prepared and homogenized overnight by magnet stirring at room temperature; subsequently, PEGDA and TMPTA cross-linkers were added to PEO solution in order to have different blends of PEO/PEGDA and PEO/TMPTA. Benzophenone 2 wt% with respect to PEO weight was added to the solution before electrospinning process. Benzophenone is a well-known photo-initiator which has two main absorption peaks at a wavelength of ~ 250 nm and ~ 350 nm.

In this work, we examined PEO/PEGDA and PEO/TMPTA blends with a similar ratio of C = C double bonds over ethylene oxide (EO) units of PEO (C = C/EO, mol/mol). The composition of the investigated samples is summarized in Table 1. Three C = C/EO ratios were used: C = C/EO = 0.065 mol/mol corresponds to the samples with the lowest amount of cross-linker (PEO/PEGDA 70/30 and PEO/TMPTA 87.5/12.5), C = C/EO = 0.15 mol/mol corresponds to the samples with the medium amount of cross-linker (PEO/PEGDA 50/50 and PEO/TMPTA 75/25), and C = C/EO = 0.35 mol/mol corresponds to the samples with the highest cross-linker content (PEO/PEGDA 30/70 and PEO/TMPTA 55/45). To simplify the samples name, the following abbreviations are used (Table 1): L-PEGDA and L-TMPTA for the lowest value of C = C/EO ratio (and thus of cross-linker), M-PEGDA and M-TMPTA for the medium C = C/EO ratio, and H-PEGDA and H-TMPTA for the highest C = C/EO ratio.

Electrospinning procedure

Electrospinning was performed by an *E*-fiber electrospinning system SKE apparatus in horizontal setup with high-voltage power supply, a programmable syringe pump (syringe tip diameter of 1 mm) and a stationary collector. Aluminum foils were used as the substrate during. Electrospinning. The electrospun mats were prepared at room temperature by applying a voltage between 8 and 12 kV (12 kV for pure PEO solutions and 8 kV for PEO/PEGDA and PEO/TMPTA solutions) and a flow rate of 0.1 ml/h, while the distance between the needle and the collector was kept 15 cm. Membranes with a thickness between 10 and 40 μm were fabricated. The thickness was measured by digital micrometer; for each sample at least 5 values in different spots of the membrane were collected and the average value was calculated.

Photo-cross-linking

Photo-curing was performed by Dymax ECE 5000 UV-Curing flood lamp. The UV lamp in this work produces UV of long wavelength from 400 to 320 nm (UV-A) and some amount of bandwidth of medium UV wavelength from 320 to 280 nm (UV-B). The samples were cured under inert atmosphere to prevent the oxygen quenching phenomena by blowing nitrogen continuously into the curing chamber. The UV light intensity was measured by an EIT radiometer and was 70 mW/cm^2 on sample surface; the time of irradiation was 20 min.

Characterization

Membrane morphology and fiber diameter were characterized by FE-SEM (Field Emission Scanning Electron Microscopy, ZEISS Supra 40). The samples were coated with a 10-nm Cr film via sputtering (by a Quorum Q150T ES sputter coater) prior to analysis.

The size distribution of fibers and the surface porosity were obtained by analyzing the FE-SEM

Table 1 Composition details of the investigated samples

Sample name	C = C/EO ratio (mol/mol)	Cross-linker	Composition	
			PEO (wt%)	Cross-linker (wt%)
L-PEGDA	0.065	PEGDA	70	30
M-PEGDA	0.15	PEGDA	50	50
H-PEGDA	0.35	PEGDA	30	70
L-TMPTA	0.065	TMPTA	87.5	12.5
M-TMPTA	0.15	TMPTA	75	25
H-TMPTA	0.35	TMPTA	55	45

images with image J software. By adjusting the grayscale threshold, binary images were obtained by having the outer layer of fibers (black foreground) in contrast with white background.

The photo-cross-linking reaction was monitored by photo-DSC measurements, performed by a Mettler Toledo DSC1 STARe system, equipped with a high-pressure mercury-xenon lamp (LIGHTNINGCURE Spotlight source LC8, Hamamatsu) with an intensity of 200 mW/cm^2. During measurement, nitrogen was continuously purged with a flux of 60 mL/min, and isothermal condition of 25 °C was maintained. The sample solution was prepared prior to the measurement and placed into the sample pan; then, pans were left in the dark at room temperature for a couple of hours for solvent evaporation. Before starting UV irradiation, samples were maintained under nitrogen flow and isothermal conditions for one minute. Afterward, the samples were irradiated and the heat flow evolution versus time throughout the photo-cross-linking reaction was monitored.

In the case of pure PEGDA and TMPTA, the photo-DSC heat evolution versus time curve was used to calculate the conversion of acrylic groups under UV irradiation. The area under the curve after subtracting the baseline was obtained; accordingly, the required energy for converting one gram of cross-linker was calculated. By considering the required energy for converting 1 mol of vinyl group as 86 kJ/mol [54], the conversion of acrylic groups in the sample was acquired.

For assessing the chemical bonds and compositions of electrospun fibers prior and after UV curing, attenuated total reflection FTIR spectroscopy (ATR-FTIR, Thermo Scientific Nicolet iS50) was used. All the spectra were normalized to the absorption at 845 cm^{-1} associated with PEO backbone, which is not affected by UV irradiation [55, 56].

Conversion was calculated by monitoring the decrease in the area A of the FTIR absorption band of the reactive functionality (acrylate C = C peak around 1640 cm^{-1}) with time t. The area was normalized by a constant signal in the spectra (C = O peak at 1720 cm^{-1}). Percent C = C conversion is given by Eq. 1:

$$\text{Conversion } \% = \left(1 - \frac{\left|A_{C=C}/A_{C=O}\right|_t}{\left|A_{C=C}/A_{C=O}\right|_{t=0}}\right) \times 100 \quad (1)$$

Three repetitions were performed, and the average conversion value and the standard deviation were calculated.

The insoluble fraction of UV-cured electrospun mats of PEO/PEGDA and PEO/TMPTA was measured by soaking the samples with a weight of 20 ± 2 mg in distilled water (which is a solvent for the uncross-linked blend) for 24 h, drying them at room temperature for 48 h and calculating the mass loss of the samples.

Dynamic Mechanical Thermal Analysis (DMTA) was performed in order to investigate the polymer structural properties. A Triton Technology instrument was used, and scans were carried out in the temperature range −100 °C–80 °C, with a heating rate of 3 °C/min, in tensile configuration at a frequency of 1 Hz. The glass transition temperature (T_g) values of the samples were measured as the maxima of tan δ.

The cross-linking density of the polymer material can be estimated by the classical rubber theory of elasticity (Eq. 2):

$$G' = vRT \quad (2)$$

where G' is the shear modulus, v is the cross-linking density (mmol/cm^3), R is the gas constant (J/(K.mol)) and T is the absolute temperature (K). Here, a temperature of 40 °C, assuring the rubbery plateau for the investigated systems, was considered for the estimation of v. G' can be written as Eq. 3, by having the Poisson ratio v_p and the storage tensile modulus E' obtained from DMTA:

$$G' = \frac{E'}{2(1+v_p)} \quad (3)$$

Poisson ratio for rubbery materials is estimated as $\sim$ 0.5, though shear can be obtained as Eq. 4:

$$G' = \frac{E'}{3} \quad (4)$$

Three replicates for each sample were measured by DMTA, and afterward, the single-factor ANOVA was performed on acquired data.

In order to study the influence of photo-cross-linking on melting temperature (T_m), T_g and degree of crystallinity, differential scanning calorimetry (DSC) was performed. The measurements were executed with a Mettler Toledo DSC1 STARe instrument. DSC analyses were carried out in 6 steps: 5 min isothermal

step at −60 °C, heating step from −60 °C to 190 °C, 5 min of isothermal phase at 190 °C, cooling step from 190 °C to −60 °C, 5 min isothermal step at −60 °C and heating to 190 °C. The heating and cooling rate was 20 °C/min. The midpoint of the increment in specific heat was recorded as the T_g, and the maxima of the melting peak in the second heating cycle was obtained as T_m. The crystallization degree (X_c) was measured by enthalpy of fusion in the second heating cycle (ΔH_f) with respect to the enthalpy of fusion for the 100% crystalline PEO (ΔH_f^0), which is 196 J/g [57], at the equilibrium melting point (T_m^0), by Eq. 5:

$$X_c = \frac{\Delta H_f(T_m)}{\Delta H_f^0(T_m^0)} \tag{5}$$

The thermal stability of the samples was analyzed by a thermogravimetric analyzer (TGA), using a Mettler Toledo TGA/SDTA 851 apparatus. Samples were heated up to 800 °C by a rate of 10 °C/min. Nitrogen flow through the furnace prevented oxidation processes, and thus, solely the thermal decomposition of samples was monitored.

The tensile strength of the samples and their elongation at break were measured using an INSTRON 3366 electromechanical universal testing machine (ITW Test and Measurement Italia S.r.l., Instron CEAST Division) equipped with a 10-kN load cell. The fibrous mats were carefully peeled off from the aluminum substrate, cut to obtain samples with dimensions of 30 mm in length, 8 mm in width and thickness of 10–40 μm and placed between the clamps. A constant stretching speed of 5 mm/min at room temperature was applied, and at least three replicates were tested for each sample. During the tensile testing, the stress (through machine-recorded force) and strain (the displacement based on initial cross-section area and gauge length) were measured and the Young's modulus E was calculated based on the initial linear elasticity regime of stress–strain curves.

The permeability of samples was evaluated by ASTM E96/E96M–16 standard [58]: the electrospun fibrous membrane was sealed to the open mouth of a test vessel containing distilled water with air space of 19 ± 6 mm from the specimen. The assembly of membrane, water and vessel was kept in controlled atmosphere (humidity = 45%, temperature = 25 °C), and the amount of water vapor transmission through the membrane was determined by periodic weighing of the assembly. The water vapor transmission (WVT) could be calculated by Eq. 6:

$$WVT = \frac{W}{tA} \tag{6}$$

in which W is weight change (g), t is time (h) and A is the test area (vessel mouth area) (m^2).

Results and discussion

In this work, as represented in Fig. 1, fibrous mats were produced by electrospinning of PEO added of two different acrylic cross-linkers, i.e., polyethylene glycol diacrylate and trimethylolpropane triacrylate. PEO/PEGDA and PEO/TMPTA blend solutions were used with different composition ratios (Table 1), after addition of a photo-initiator. Then, the fibrous mats were irradiated to promote radical curing of the material, exploiting both the high reactivity of the acrylic groups of the multifunctional cross-linker and the photo-induced hydrogen abstraction reaction from PEO [56]. Cross-linking was used to enhance the properties (e.g., chemical, thermal and mechanical properties) of the nanofibrous membranes, in particular their solvent resistance, and thus enlarge their applicability. The fiber fabrication and the membrane morphology, the kinetics of the cross-linking reaction as well as the photo-cross-linking efficiency were studied. Moreover, the fibrous membranes were characterized in terms of thermal and mechanical properties, water resistance and permeability. In particular, the effect of the type (difunctional PEGDA or trifunctional TMPTA) and amount of cross-linker was evaluated.

Electrospun mat morphology

The morphology of photo-cured PEO/PEGDA and PEO/TMPTA fiber mats was analyzed by FE-SEM. As observed in Fig. 2a, the presence of both cross-linkers did not interfere with the fiber formation during electrospinning; thus, fibrous membranes were obtained with all starting solutions. However, the photo-cured PEO/PEGDA mats showed regions of un-homogeneity along the single fiber, whereas the PEO/TMPTA mats were more uniform and defect-free.

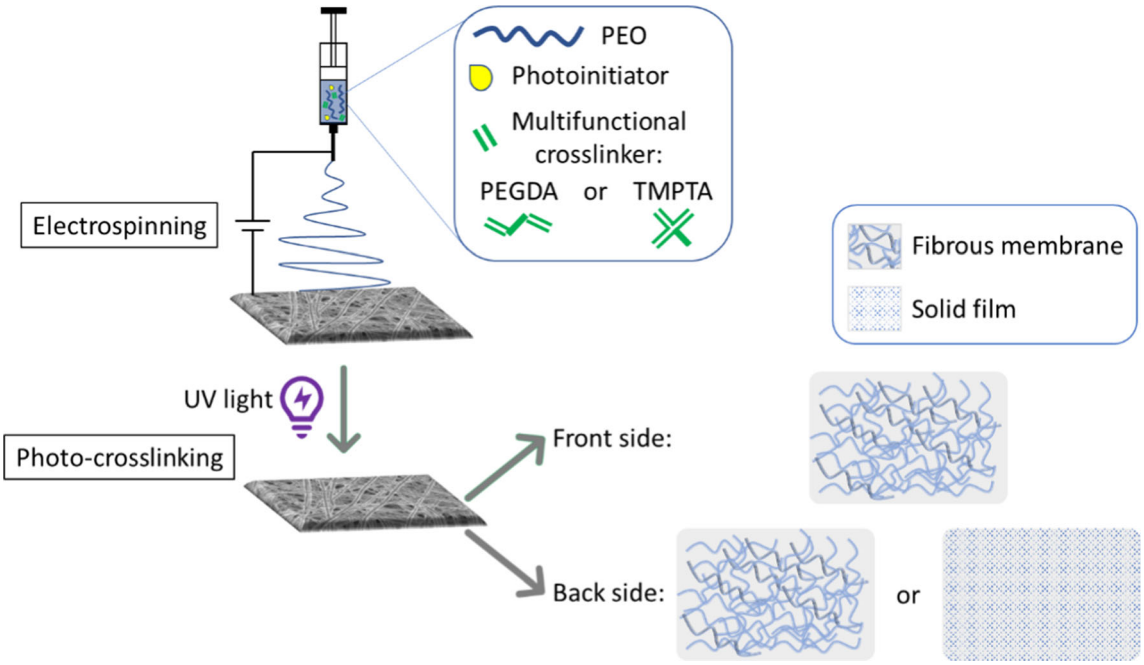

Figure 1 Scheme of the electrospinning process coupled with photo-cross-linking of PEO/cross-linker blends to obtain photo-cured fibrous membranes.

In order to check the uniformity of the membranes along their thickness, they were analyzed also on their back side (Fig. 2b), by carefully peeling them off from the collector and imaging them by FE-SEM, as sketched in Fig. 1. As shown in Fig. 2, PEO/PEGDA mats have a totally different morphology on the two sides: with the lower amount of cross-linker (L-PEGDA), connections among fibers are formed on the bottom part of the mat, while with the medium and highest amount of cross-linker (M-PEGDA and H-PEGDA) a semi-film is produced and the fiber morphology is even completely lost on the back side. This is likely due to the high content of liquid cross-linker in the electrospinning solution (i.e., 50 and 70 wt% for M-PEGDA and H-PEGDA, respectively), which can flow toward the bottom layer of the membrane prior to solidification by the photo-curing reaction. As shown in Fig. 2, the electrospun mats containing TMPTA as cross-linker are more uniform along their thickness and the nanofibrous morphology is maintained on both sides, independently on the amount of cross-linker used. In fact, in these cases, the content of liquid TMPTA in the electrospinning solution is lower, ranging from 12.5 to 45 wt% (Table 1), and the cross-linker viscosity is higher.

Figure 2c reports the size distribution of the electrospun fibers, measured on the top surface (front side): it can be seen that samples containing PEGDA show a wider range of size distribution, while those with TMPTA are more uniform and resulted in a narrower size distribution window. Also this effect could be ascribed to the fact that liquid PEGDA tends to flow after electrospinning and prior to photo-curing. Moreover, the fibers containing TMPTA as cross-linker are thinner; homogeneous photo-cured membranes with an average fiber diameter of 320 ± 30 nm were obtained.

The surface porosity of the membranes was evaluated by performing image processing on the FE-SEM images: data are reported in Fig. 2d. The PEO/PEGDA front side has quite high surface porosity, while the back side looks more like a film rather than a fibrous membrane (very low porosity): the difference of surface porosity between the two sides of the mat is at least 20 percentage points. Dissimilarly, the PEO/TMPTA samples are much more uniform and show a fibrous surface with a porosity of around 30% on both sides; porosity is independent of the TMPTA content.

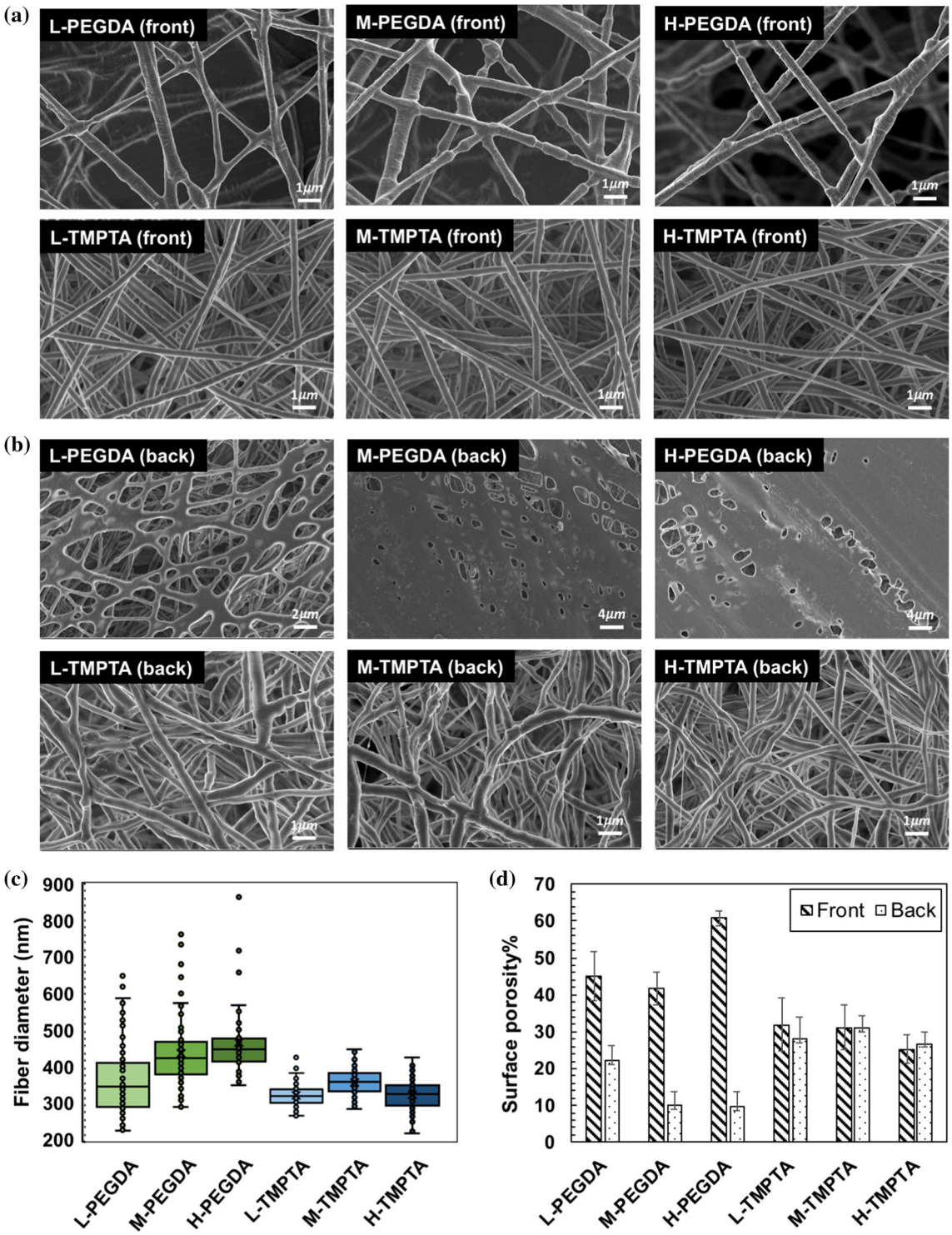

Figure 2 Morphology of the PEO-based photo-cured electrospun fibrous mats with different types of cross-linker and different composition ratios of PEO/cross-linker (L-PEGDA, M-PEGDA, H-PEGDA and L-TMPTA, M-TMPTA, H-TMPTA). **a** FE-SEM images of the front side (top surface) of the membranes. **b** FE-SEM images of the back side (bottom surface) of the membranes. **c** Fiber diameters distribution of the top surface of the electrospun mats. **d** Surface porosity of both sides of the fibrous membranes.

Photo-curing of the fibrous mats

The photo-curing reaction and its efficiency were monitored and analyzed by photo-DSC, FTIR spectroscopy and the measurement of the insoluble fraction.

The generated heat rate during photo-cross-linking can be considered proportional to the kinetics of the reaction, including the initiation, propagation and termination stages. Accordingly, photo-DSC was carried out in isothermal conditions for measuring the exothermic heat of photo-cross-linking reaction over time for all blends as well as for pure PEO, PEGDA and TMPTA. As shown in Fig. 3, all samples alongside PEO alone, PEGDA alone and TMPTA alone show the typical curve trend of a photo-cross-linking reaction, including the initiation or activation of the excited species, the propagation of cross-linking reaction between the excited molecules and the termination of reaction.

Neat PEO sample as a solid required a very long curing time before reaching a plateau phase: in the very first minutes of reaction the peak of heat flow depending on radical formations along the PEO chain was developed, and then, a long tail of slow termination phase was followed. The reaction continued till 2 h before a stable regime was reached (data not shown). The photo-cross-linking reaction of neat PEGDA and TMPTA instead reached a plateau phase very fast (in the range of few minutes), after the exothermic peak of reaction. This peak is much more pronounced (i.e., higher amount of heat generated) for PEGDA than for TMPTA.

The PEO/PEGDA samples showed a highly accelerated reaction with respect to PEO, dependent on PEGDA content in the formulation. In fact, as can be clearly seen in the inset of Fig. 3, higher the amount of PEGDA in the formulation sharper the heat flow peak, and higher the PEO content longer the reaction tail. It is important to notice that the peak of heat flow is associated with both PEO and PEGDA reactions and cannot be considered solely as a heat of conversion of PEGDA species.

For PEO/TMPTA samples, different photo-curing kinetics results were obtained. Firstly, the reaction was not as fast as that of PEO/PEGDA systems, and a lower amount of heat was generated during the photo-cross-linking. This means that the conversion of TMPTA reactive groups proceeds with a lower extent compared to PEGDA: in fact, after 5 min of irradiation, the acrylic groups conversion was found approximately 13% and 82% for TMPTA and PEGDA cross-linker, respectively. The low acrylic conversion degree of TMPTA-containing samples was confirmed also by ATR-FTIR analyses on cured polymer after photo-DSC. Moreover, the effect of the cross-linker content on the reaction kinetics is the opposite for PEO/TMPTA samples, compared to PEO/PEGDA samples. As PEO reacts faster than TMPTA and slower than PEGDA, lower the amount of TMPTA in the formulation sharper the heat flow peak. As expected, L-TMPTA resulted in slower reaction demanding higher energy for evolution and more

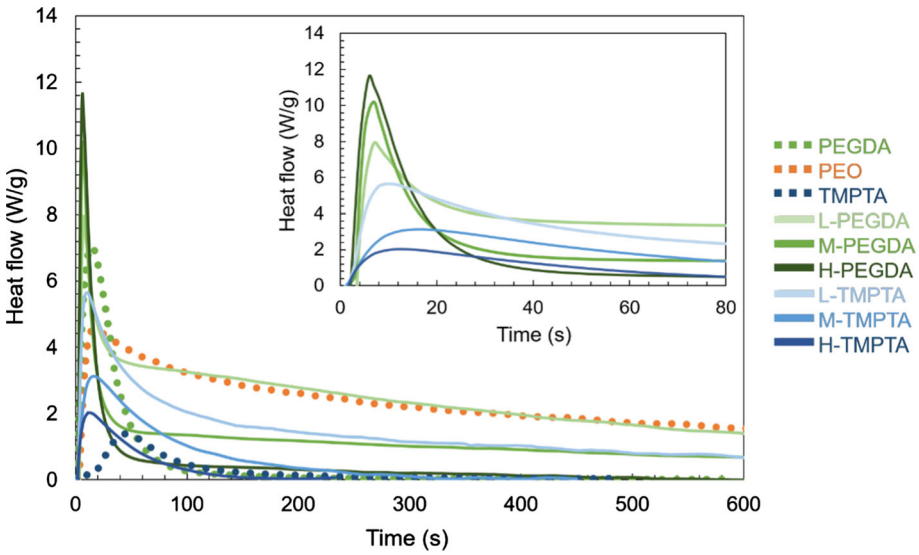

Figure 3 Photo-DSC of PEO/PEGDA and PEO/TMPTA blends as well as pure PEO, pure PEGDA and pure TMPTA, in the presence of photo-initiator, at isothermal condition of 25 °C under inert atmosphere of N_2 and irradiation with light intensity of 200 mW/cm^2. The inset reports the photo-DSC curves for the first 80 s of irradiation.

similar to PEO developing pattern, while H-TMPTA showed a very similar behavior to pure TMPTA.

Quantitatively studying the enthalpy of reaction, it can be calculated that the slow photo-cross-linking of pure PEO produces ~ 3000 J/g (in 80 min of irradiation), while the faster reaction of PEGDA develops only ~ 244 J/g and that of TMPTA ~ 110 J/g (in 200 and 300 s of irradiation, respectively) before reaching the plateau state. For samples of PEO/cross-linker, the reaction is more complex than in the case of only one reacting species: different competing reactions can take place at the same time, meaning PEO-cross-linker, PEO-PEO, cross-linker–cross-linker reactions.

Analyzing the photo-DSC results, it is clear that in the case of PEO/PEGDA and PEO/TMPTA blends, the irradiation time required for assuring a sufficient cross-linking reaction without degrading the material is around 7 min; thus, the UV dose (defined as the product of light intensity and the irradiation time) corresponds to 84 J/cm^2. In the following, this dose was used to cross-link the fibrous membranes.

The chemical structure of the electrospun fibrous membranes prior and post-photo-curing was controlled through ATR-FTIR spectroscopy (Fig. 4). As an example, Fig. 4a shows the FTIR spectra of the blend fibrous mats with the highest content of cross-linker before curing (uncured H-PEGDA and H-TMPTA) and after curing (UV-cured H-PEGDA and H-TMPTA). The spectrum of pure PEO is also reported as reference. In the PEO/cross-linker blend mats, the peaks arising from PEO were found at 2876 cm^{-1} (C–H stretching), 1466 cm^{-1} (C–H bending); 1360 cm^{-1} and 1341 cm^{-1} (CH_2 wagging), 1279 cm^{-1} (CH_2 twisting), 1145 cm^{-1}, 1100 cm^{-1} and 1060 cm^{-1} (triplet peak due to C–O–C absorption complex). In PEO/PEGDA samples, the characteristic peaks of PEGDA were found at 1638 cm^{-1} (double peak due to the stretching of vinyl groups), and 910 cm^{-1} and 1720 cm^{-1} (C = O absorption band). Similarly, characteristics peaks of TMPTA were found for PEO/TMPTA samples at 1638 cm^{-1} (vinyl groups) and 1720 cm^{-1} (intense carbonyl peak).

The UV-cured fibrous mats showed a small shift of few wavenumbers of all peaks, but a degradation of the PEO component could not be detected. The decrease with UV irradiation of the peak at 1638 cm^{-1} related to C = C reactive groups (Fig. 4b) is evident. The C = C double bond conversion after photo-curing was calculated (Fig. 4c) and resulted to be 70–80% for PEO/PEGDA and 40–45% for PEO/TMPTA samples. The C = C conversion in samples containing TMPTA is much lower than in those containing PEGDA as cross-linker, although the FE-SEM images and the gel content results (discussed below) confirmed the successful cross-linking of the material. Considering the branched structure of tri-functional TMPTA in comparison with the linear structure of difunctional PEGDA, we can presume that some of the TMPTA double bonds did not react due to their position in the polymer structure or in the fiber, while a sufficient amount took part to the reaction and formed the cross-linked network.

The gel content of the cured fibrous mats of PEO/PEGDA and PEO/TMPTA was measured by immersing them in distilled water (which is a good solvent for uncured PEO polymer, and for PEGDA and TMPTA monomers). Table 2 shows that the weight loss of the samples varies from 8% to nearly 33% depending on the cross-linker content. For all investigated samples, the insoluble fraction increases with the amount of cross-linker. For the fibers containing PEGDA in initial formulation, this increase is very low: the membranes showed a comparable gel content for medium and high cross-linker values (M-PEGDA and H-PEGDA) and a slightly lower value for the lowest amount of PEGDA (L-PEGDA). Instead, the fibrous membranes containing TMPTA showed larger changes of insoluble fraction percentage by adding cross-linker, from 68 to 92% for L-TMPTA and H-TMPTA, respectively. It can be concluded that, in case of L-TMPTA, although there should be enough number of acrylic groups for a complete cross-linking reaction, many of them do not react during UV curing, and as a result, the uncross-linked portion of the sample can be dissolved in water and washed away.

By performing DMTA, it is possible to evaluate the cross-linking density ν of photo-cured films, as described in "Experimental" section. By considering the PEO-based fibrous membranes as plain films, the classic rubbery theory can be applied and the cross-linking density calculated. However, it should be noted that the electrospun membranes are porous structures, and thus, the measure of ν can be used only as rough estimation.

First, all the PEO/PEGDA and PEO/TMPTA cross-linked mats showed a rubbery plateau regime after the glass transition, which confirmed the cross-linking efficiency. For all samples, the cross-linking

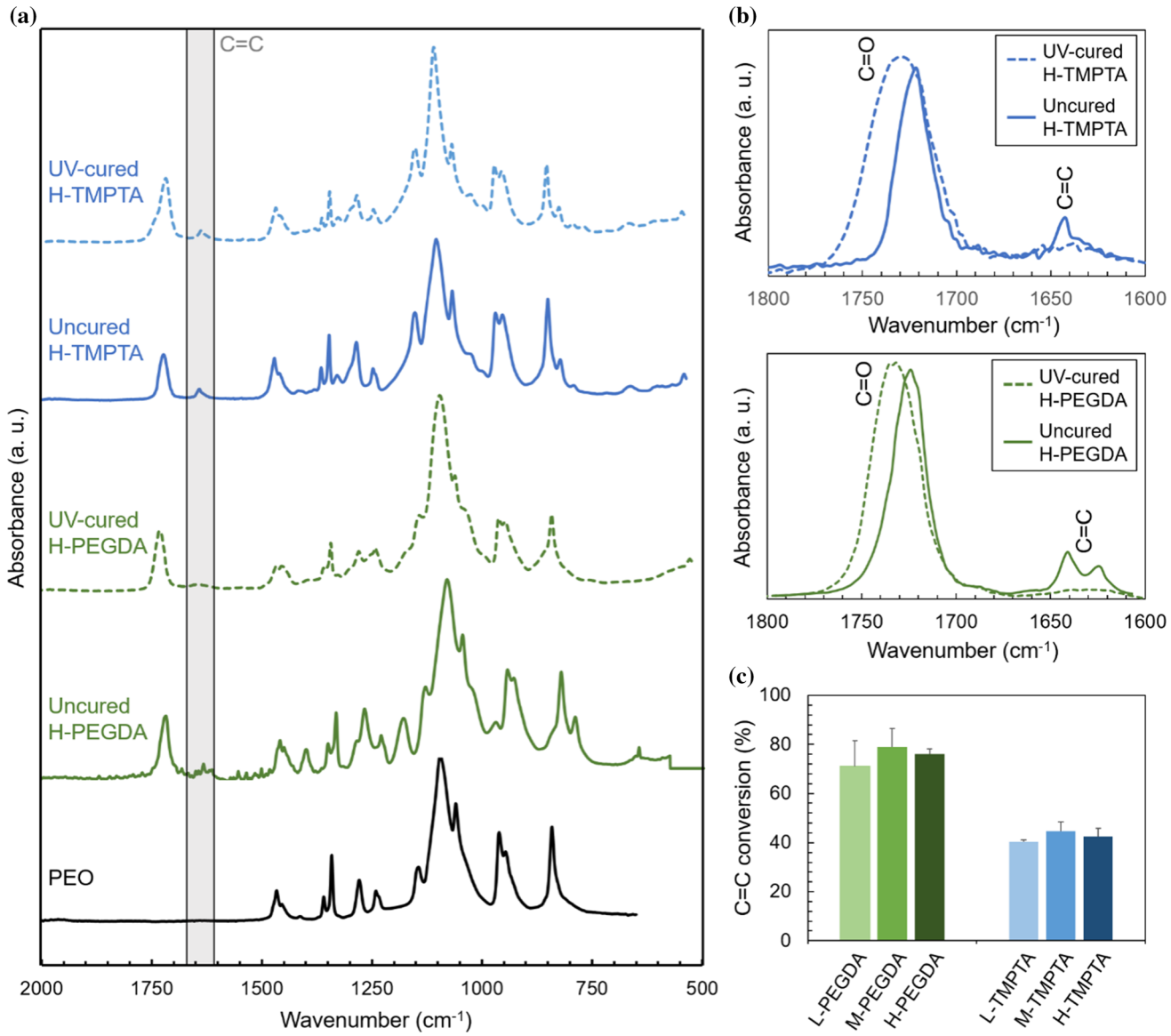

Figure 4 ATR-FTIR spectroscopic analyses. **a** Spectra of pure PEO, and of H-PEGDA and H-TMPTA electrospun fibrous membranes prior (uncured) and after (UV-cured) UV irradiation. **b** Details of the spectra in the range 1600–1800 cm^{-1} showing the reduction in the peak due to double bonds (C = C) after UV curing. **c** C = C conversion for PEO/PEGDA and PEO/TMPTA electrospun fiber membranes.

Table 2 Insoluble fraction of PEO/PEGDA and PEO/TMPTA photo-cured fibrous membranes

Sample	Insoluble fraction (%)
L-PEGDA	76.4 ± 1.8
M-PEGDA	87.4 ± 2.8
H-PEGDA	88.3 ± 2.6
L-TMPTA	67.7 ± 0.5
M-TMPTA	76.0 ± 3.3
H-TMPTA	92.0 ± 2.0

density was in the range 10^{-3}–10^{-2} mol/cm^3 (Table S1 in the Electronic Supplementary Material, ESM), thus proving that the electrospun membranes are adequately cross-linked. The one-way ANOVA on different measurement results showed that all obtained values of v belong to the same group of data, and thus, they cannot be differentiated based on cross-linker type or on the ratio of double bonds to ethoxy group C = C/EO (i.e., cross-linker amount).

Characterization of the photo-cured fibrous mats

The thermal properties of the fibrous mats were assessed by DMTA, DSC and TGA. In Table 3, the T_g values obtained by DMTA are reported. The T_g of uncured PEO was found at −53 °C. The three fibrous mats of PEO/PEGDA showed a T_g with increased values by increasing the cross-linker amount. The PEO/TMPTA samples also showed higher T_g with respect to PEO, but with an opposite trend of the effect of the cross-linker amount. Interestingly, a double T_g transition was detected for M-PEGDA and H-PEGDA samples, indicating the presence of two different species in the membranes. This is most likely due to the flowing of liquid PEGDA and consequent phase separation that occurs prior to photo-curing: the mat top surface is mainly formed by PEO fibers, while the bottom layer is a semi-film primarily containing photo-cured PEGDA.

The glass transition temperature of all samples was confirmed by DSC analyses, which provided also the melting temperature of the polymers. For different samples (i.e., L-PEGDA, M-PEGDA, H-PEGDA and H-TMPTA), the DSC analysis showed the existence of two T_ms (Table 3 and Fig. S1 in ESM). In fact, in these cases the second DSC heating cycle revealed an endothermic double peak, in which one maximum is close to the PEO melting temperature (64 °C) and the other is found at lower temperature. This second maximum can be associated with the variation in microstructure due to the cross-linked portion of the sample.

The degree of crystallinity of the photo-cross-linked blend samples was evaluated by DSC analyses (Table 3). They showed a reduced crystallinity with respect to pure PEO (63% of crystallinity), as expected considering that only the long PEO chains can crystallize, whereas PEGDA and TMPTA networks are amorphous. However, it is important to notice that the crystallinity of PEO/PEGDA and PEO/TMPTA cross-linked fibrous membranes is comparable with the theoretical values calculated considering the PEO content in the initial electrospinning formulation (Table 3). Therefore, neither the electrospinning process nor the network formation through photo-cross-linking hindered the PEO crystallinity.

The thermal resistance of the photo-cured fibrous mats was evaluated by TGA; the thermograms are reported in Fig. S2 of the ESM and the main results in Table 3. According to the first derivative of the TGA curves the decomposition peak occurred at a similar temperature T_d for all samples: the cross-linked systems showed the main thermal degradation at around 407 °C, a slightly greater value compared with pure PEO fibers. Concerning the T_{10} (i.e., the temperature at which the sample loses 10% of its initial weight) values, they decrease by adding the cross-linker. The lower temperature of onset of degradation can arise from residual cross-linker content in the system that has not reacted during irradiation.

The mechanical properties of the photo-cured fibrous membranes were investigated by tensile tests (Fig. 5). The Young's modulus E was obtained from the linear regime of the stress–strain curves. The obtained values are in agreement with the literature regarding PEO electrospun mats [35, 50]. All PEO/cross-linker membranes exhibited elastic deformation without undergoing permanent deformation before their failure. However, the two sets of investigated samples (i.e., membranes containing PEGDA and

Table 3 Thermal properties of PEO/PEGDA and PEO/TMPTA photo-cured fibrous membranes, as well as pure PEO, obtained by DMTA, DSC and TGA analyses

Sample	T_g (°C) by DMTA	T_m (°C) by DSC	Theoretical degree of crystallinity (%)	Degree of crystallinity (%) by DSC	T_d (°C) by TGA	T_{10} (°C) by TGA
PEO	−53	64	–	62.9	399	380
L-PEGDA	−30.2	61.7 55.3	44.0	39.74	408	368
M-PEGDA	−27 −21.7	62 55.5	31.4	23.99	401	345
H-PEGDA	−24.7 −19	62.7 56.3	18.9	22.63	400	351
L-TMPTA	−34.4	63.48	55.0	61.19	408	358
M-TMPTA	−35.4	61.1	47.2	55.34	418	364
H-TMPTA	−47.6	56.15 48.58	34.6	33.22	408	356

TMPTA) showed different behaviors. The sample L-PEGDA exhibited lower tensile modulus and quite higher elongation at the breaking point. The samples M-PEGDA and H-PEGDA, with higher modulus by nearly one order of magnitude, presented reduced extension ability due to a more cross-linked network with lower elastic characteristics. The values obtained for M-PEGDA and H-PEGDA can be ascribed to the formation of a semi-continuous highly cross-linked film on the bottom surface of the membranes. On the contrary, the PEO/TMPTA samples showed a slightly decrease in E value (from 17 to 12 MPa) and an increase in elongation capacity (from 9 to 26%) by increasing the TMPTA amount in the initial formulation.

The permeability of the fibrous membranes was obtained by periodic gravimetric method. The weight of the test assembly and accordingly the water vapor transmission was controlled for two weeks. As shown in Fig. 6, for PEO/PEGDA membranes the samples containing the most amount of cross-linker have the highest value of WVT, followed by medium and lowest content of cross-linker. The highest permeability of M-PEGDA and H-PEGDA can be correlated with the higher surface porosity of the top layer of the mats, while the packed backside of the samples seems to not interfere with their permeability properties. PEO/TMPTA fibrous membranes showed instead all a similar water permeability, as their surface porosity is independent on the amount of cross-linker. The obtained permeability values, in the range 900–1030 g.day^{-1} m^{-2}, make cross-linked electrospun fibrous mat as breathable membranes.

In order to control the water resistance of the photo-cured membranes (including their fibrous morphology retention), they were subjected to aqueous medium and left to get dried prior to FE-SEM imaging. It is known that if a uncross-linked PEO electrospun mat is immersed in water, first its fiber morphology is lost (i.e., a continuous film is formed), and then, the polymer is completely dissolved. As shown in Fig. 7, all the PEGDA-containing samples

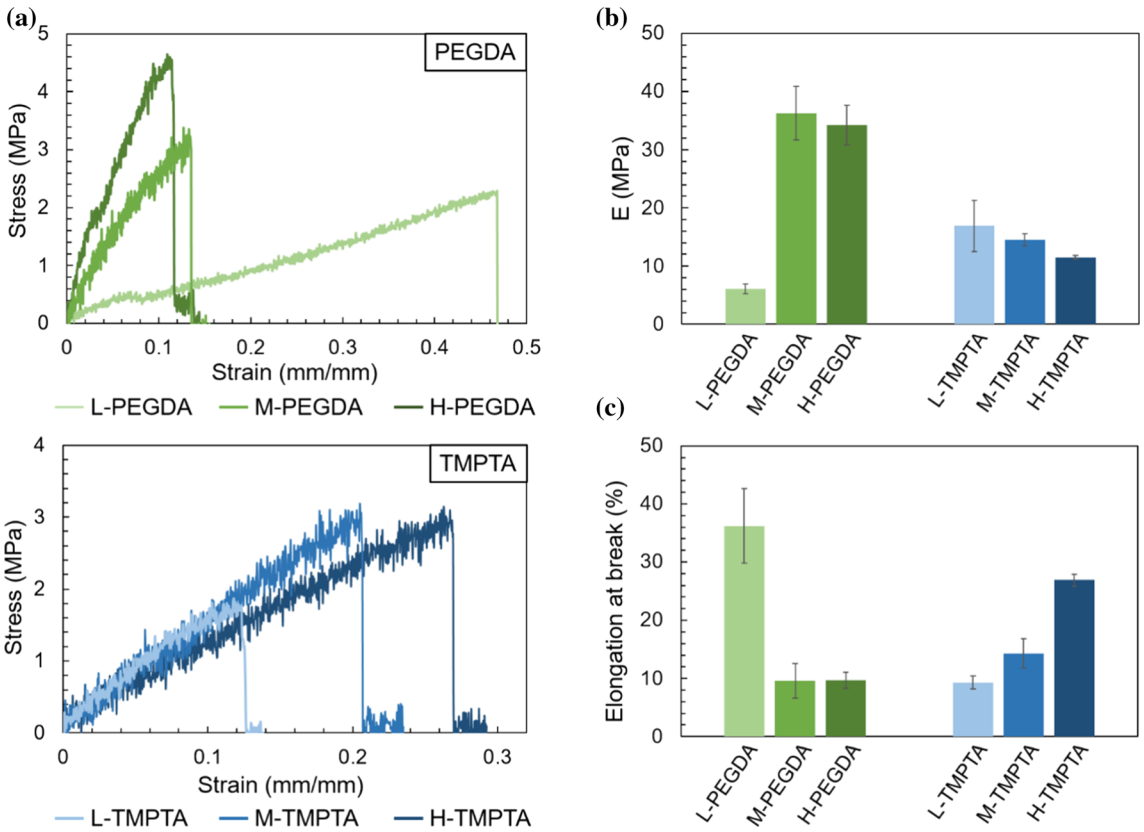

Figure 5 Mechanical tensile characterization of photo-cured fibrous mats of PEO/PEGDA and PEO/TMPTA. **a** Stress *vs.* strain curves; one curve for each sample is reported as an example. **b** Young's modulus E values obtained from the linear regime of the curves in **(a)**. **c** Elongation at break values, measured from the curves in **(a)**. The error bars in **(b)** and **(c)** were calculated performing at least three replicates for each sample.

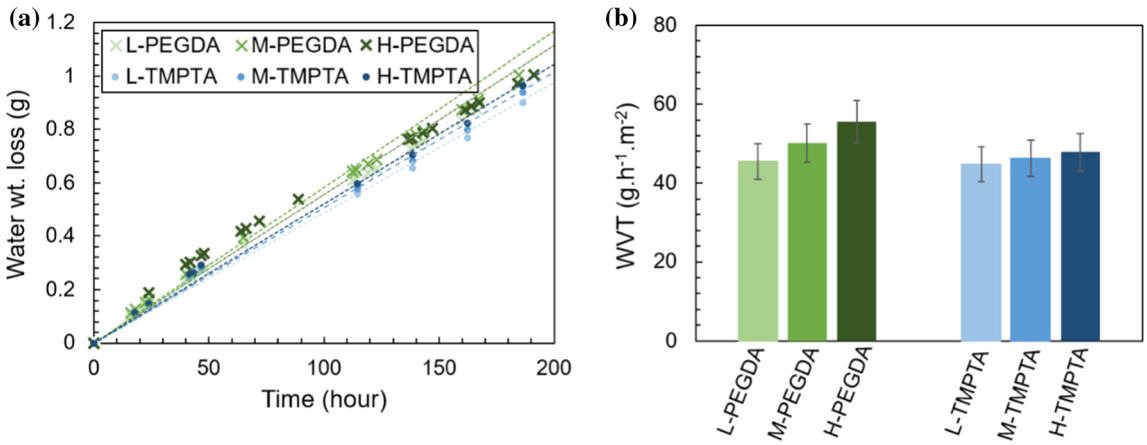

Figure 6 Water permeability of the photo-cured electrospun membranes of PEO/PEGDA and PEO/TMPTA. **a** Water weight loss as a function of time. **b** Average measurement of the water vapor transmission WVT after two weeks.

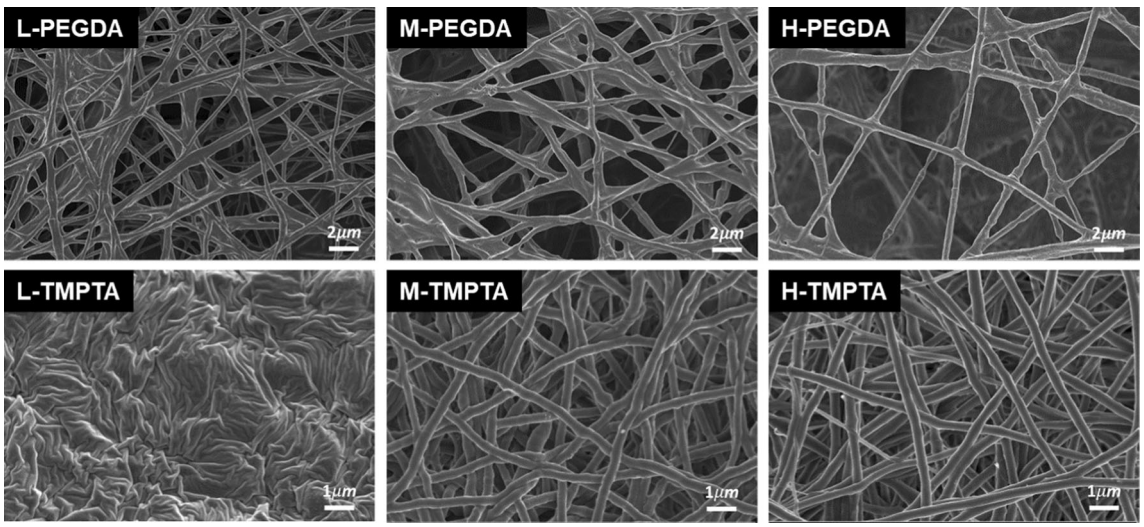

Figure 7 FE-SEM images of the photo-cured electrospun fibrous membranes of PEO/PEGDA and PEO/TMPTA after water treatment.

showed fibers morphology even after water treatment, whereas, apparently, 12.5 wt% of TMPTA (L-TMPTA) was not sufficient for creating water-resistant fibrous mats, although a similar ratio of vinyl groups to the EO moiety based on initial formulation was used as for L-PEGDA. Instead, both M-TMPTA and H-TMPTA retained their homogeneous fibrous morphology after water treatment and no change in the fibers size was detected. Therefore, these two systems allowed to form uniform nanofibrous mats with superior water resistance by applying photo-curing after the electrospinning process, paving the way for a wider application of PEO-based membranes.

Conclusions

This study presents a method to fabricate modified electrospun PEO-based fibrous membranes with enhanced properties and with superior water resistance, the obstacle that generally hinders the application of PEO fibers in different fields. By adding a multifunctional cross-linker to the electrospinning solution and applying UV curing to the electrospun mat, a cross-linked network is formed. Two cross-linkers were employed, namely PEGDA and TMPTA, and different acrylic groups/PEO ratios were tested. The membrane morphology was investigated by FE-SEM: when PEGDA is used, only the upper surface of

the mat is formed by nanofibers and the bottom layer is a semi-continuous film, whereas when TMPTA is used homogeneous fibrous membranes with an average fiber diameter of 320 nm are obtained. The kinetics of photo-cross-linking reaction was studied through photo-DSC, and an acceleration of the reaction was observed when the cross-linker was added; however, the reaction showed a complex nature due to the presence of two concomitant reactive species (i.e., PEO and the cross-linker). FTIR spectroscopy and insoluble fraction measurements confirmed the successful cross-linking of the electrospun membranes.

The effect of the type and amount of cross-linker on the thermal, mechanical and permeability properties of the photo-cured fibrous membranes was evaluated. More importantly, it was demonstrated that their fibrous morphology is completely maintained after water treatment, especially when 25 wt%–45 wt% of TMPTA were used. This feature can highly widen the application fields of PEO-based fibrous membranes, especially in the water treatment and biomedical areas.

Funding

Open access funding provided by Politecnico di Torino within the CRUI-CARE Agreement.

Electronic supplementary material: The online version of this article (https://doi.org/10.1007/s10853-020-05346-3) contains supplementary material, which is available to authorized users.

Open Access This article is licensed under a Creative Commons Attribution 4.0 International License, which permits use, sharing, adaptation, distribution and reproduction in any medium or format, as long as you give appropriate credit to the original author(s) and the source, provide a link to the Creative Commons licence, and indicate if changes were made. The images or other third party material in this article are included in the article's Creative Commons licence, unless indicated otherwise in a credit line to the material. If material is not included in the article's Creative Commons licence and your intended use is not permitted by statutory regulation or exceeds the permitted use, you will need to obtain permission directly from the copyright holder. To view a copy of this licence, visit http://creativecommons.org/licenses/by/4.0/.

References

[1] Li D, Xia Y (2004) Electrospinning of nanofibers: reinventing the wheel? Adv Mater 16:1151–1170. https://doi.org/10.1002/adma.200400719

[2] Reneker DH, Chun I (1996) Nanometre diameter fibres of polymer, produced by electrospinning. Nanotechnology 7:216. https://doi.org/10.1088/0957-4484/7/3/009

[3] Rieger KA, Birch NP, Schiffman JD (2013) Designing electrospun nanofiber mats to promote wound healing–a review. J Mater Chem B 1:4531–4541. https://doi.org/10.1039/C3TB20795A

[4] Vasita R, Katti DS (2006) Nanofibers and their applications in tissue engineering. Int J Nanomed 1:15. https://doi.org/10.2147/nano.2006.1.1.15

[5] Bhardwaj N, Kundu SC (2010) Electrospinning: a fascinating fiber fabrication technique. Biotechnol Adv 28:325–347. https://doi.org/10.1016/j.biotechadv.2010.01.004

[6] Leidy R, Ximena Q-CM (2019) Use of electrospinning technique to produce nanofibres for food industries: a perspective from regulations to characterisations. Trends Food Sci Technol 85:92–106

[7] Niu G, Zhang H, Song L, Cui X, Cao H, Zheng Y, Zhu S, Yang Z, Yang H (2008) Thiol/acrylate-modified PEO-PPO-PEO triblocks used as reactive and thermosensitive copolymers. Biomacromol 9:2621–2628. https://doi.org/10.1021/bm800573e

[8] Yang T, Zhan L, Huang CZ (2020) Recent insights into functionalized electrospun nanofibrous films in chemo-/biosensors. TrAC Trends Anal Chem. https://doi.org/10.1016/j.trac.2020.115813

[9] Sill TJ, von Recum HA (2008) Electrospinning: applications in drug delivery and tissue engineering. Biomaterials 29:1989–2006. https://doi.org/10.1016/j.biomaterials.2008.01.011

[10] Xu X, Wang H, Jiang L, Wang X, Payne SA, Zhu JY, Li R (2014) Comparison between cellulose nanocrystal and cellulose nanofibril reinforced poly(ethylene oxide) nanofibers and their novel shish-kebab-like crystalline structures. Macromolecules 47:3409–3416. https://doi.org/10.1021/ma402627j

[11] J. Doshi, D.H. Reneker, Electrospinning process and applications of electrospun fibers, In: Conf rec 1993 IEEE ind

appl conf twenty-eighth IAS annu meet IEEE 1993: pp. 1698–1703.

[12] Soares RMD, Siqueira NM, Prabhakaram MP, Ramakrishna S (2018) Electrospinning and electrospray of bio-based and natural polymers for biomaterials development. Mater Sci Eng C 92:969–982. https://doi.org/10.1016/j.msec.2018.08.004

[13] Kianfar P, Vitale A, Dalle Vacche S, Bongiovanni R (2019) Photo-crosslinking of chitosan/poly(ethylene oxide) electrospun nanofibers. Carbohydr Polym 217:144–151

[14] Sridhar R, Lakshminarayanan R, Madhaiyan K, Barathi VA, Hsiu K, Lim C, Ramakrishna S (2015) Chem soc rev nanofibers based on natural materials : applications in tissue regeneration, drug delivery. Chem Soc Rev 44:790–814. https://doi.org/10.1039/C4CS00226A

[15] Song X, Dong P, Gravesande J, Cheng B, Xing J (2018) UV-mediated solid-state cross-linking of electrospinning nanofibers of modified collagen. Int J Biol Macromol 120:2086–2093. https://doi.org/10.1016/j.ijbiomac.2018.09.029

[16] Vitale A, Massaglia G, Chiodoni A, Bongiovanni R, Pirri CF, Quaglio M (2019) Tuning porosity and functionality of electrospun rubber nanofiber mats by photo-crosslinking. ACS Appl Mater Interfaces 11:24544–24551. https://doi.org/10.1021/acsami.9b04599

[17] Theron SA, Zussman E, Yarin AL (2004) Experimental investigation of the governing parameters in the electrospinning of polymer solutions. Polymer (Guildf) 45:2017–2030

[18] Thompson CJ, Chase GG, Yarin AL, Reneker DH (2007) Effects of parameters on nanofiber diameter determined from electrospinning model. Polymer (Guildf) 48:6913–6922. https://doi.org/10.1016/j.polymer.2007.09.017

[19] Beachley V, Wen X (2009) Effect of electrospinning parameters on the nanofiber diameter and length. Mater Sci Eng C 29:663–668. https://doi.org/10.1007/s40204-017-0071-0

[20] Harris JM (2013) Poly (ethylene glycol) chemistry: biotechnical and biomedical applications. Springer, USA

[21] Bailey FEJ (2012) Poly (ethylene oxide). Academic Press, London

[22] Xu F, Gough I, Dorogin J, Sheardown H, Hoare T (2020) Nanostructured degradable macroporous hydrogel scaffolds with controllable internal morphologies via reactive electrospinning. Acta Biomater. https://doi.org/10.1016/j.actbio.2019.12.038

[23] Rajam S, Ho C-C (2006) Graft coupling of PEO to mixed cellulose esters microfiltration membranes by UV irradiation. J Memb Sci 281:211–218. https://doi.org/10.1016/j.memsci.2006.03.034

[24] Aqil A, Vasseur S, Duguet E, Passirani C, Benoît J-P, Roch A, Müller R, Jérôme R, Jérôme C (2008) PEO coated magnetic nanoparticles for biomedical application. Eur Polym J 44:3191–3199. https://doi.org/10.1016/j.eurpolymj.2008.07.011

[25] Fusco S, Borzacchiello A, Netti PA (2006) Perspectives on: PEO-PPO-PEO triblock copolymers and their biomedical applications. J Bioact Compat Polym 21:149–164. https://doi.org/10.1177/0883911506063207

[26] Patanaik A, Jacobs V, Anandjiwala RD (2010) Performance evaluation of electrospun nanofibrous membrane. J Memb Sci 352:136–142. https://doi.org/10.1016/j.memsci.2010.02.009

[27] Liu SL, Shao L, Chua ML, Lau CH, Wang H, Quan S (2013) Recent progress in the design of advanced PEO-containing membranes for CO2 removal. Prog Polym Sci 38:1089–1120. https://doi.org/10.1016/j.progpolymsci.2013.02.002

[28] Stringer JL, Peppas NA (1996) Diffusion of small molecular weight drugs in radiation-crosslinked poly(ethylene oxide) hydrogels. J Control Release 42:195–202. https://doi.org/10.1016/0168-3659(96)01457-5

[29] Pielichowska K, Głowinkowski S, Lekki J, Biniaś D, Pielichowski K, Jenczyk J (2008) PEO/fatty acid blends for thermal energy storage materials structural/morphological features and hydrogen interactions. Eur Polym J 44:3344–3360

[30] Deng F, Wang X, He D, Hu J, Gong C, Ye YS, Xie X, Xue Z (2015) Microporous polymer electrolyte based on PVDF/PEO star polymer blends for lithium ion batteries. J Memb Sci 491:82–89. https://doi.org/10.1016/j.memsci.2015.05.021

[31] Zhong SP, Zhang YZ, Lim CT (2010) Tissue scaffolds for skin wound healing and dermal reconstruction. Wiley Interdiscip Rev Nanomed Nanobiotechnology 2:510–525. https://doi.org/10.1002/wnan.100

[32] Teixeira RSP, Correa RJ, Belvino A, Nascimento RSV (2013) UV irradiation-induced crosslinking of aqueous solution of poly(ethylene oxide) with benzophenone as initiator. J Appl Polym Sci 130:2458–2467. https://doi.org/10.1002/app.39381

[33] Perloni P, Magistris A, Chiodelli G, Faucitano A, Buttafava A (1991) Effects of gamma-radiation on polymer electrolytes: PEO and PEO20-LiClO4. Int J Radiat Appl Instrum Part C Radiat Phys Chem 37:615–621

[34] F.L. Villain, J.-M.A. Parel, W.G. Lee, G. Simon Injectable polyethylene oxide gel implant and method for production. US Patent 5645583 (1997).

[35] Zhou C, Wang Q, Wu Q (2012) UV-initiated crosslinking of electrospun poly (ethylene oxide) nanofibers with

pentaerythritol triacrylate: effect of irradiation time and incorporated cellulose nanocrystals. Carbohydr Polym 87:1779–1786. https://doi.org/10.1016/j.carbpol.2011.09.095

[36] Sloop SE, Lerner MM, Stephens TS, Tipton AL, Paull DG, Stenger-Smith JD (1994) Cross-linking poly (ethylene oxide) and poly [oxymethylene-oligo (oxyethylene)] with ultraviolet radiation. J Appl Polym Sci 53:1563–1572. https://doi.org/10.1002/app.1994.070531202

[37] Şimşek M, Çakmak S, Gümüşderelioğlu M (2016) Insoluble poly(ethylene oxide) nanofibrous coating materials: effects of crosslinking conditions on the matrix stability. J Polym Res. https://doi.org/10.1007/s10965-016-1127-x

[38] Padmavathi NC, Chatterji PR (1996) Structural characteristics and swelling behavior of poly (ethylene glycol) diacrylate hydrogels. Macromolecules 29:1976–1979. https://doi.org/10.1021/ma950827r

[39] Emami SH, Salovey R (2003) Crosslinked poly (ethylene oxide) hydrogels. J Appl Polym Sci 88:1451–1455. https://doi.org/10.1002/app.11813

[40] Tonda-Turo C, Ruini F, Ramella M, Boccafoschi F, Gentile P, Gioffredi E, G. Falvo D'Urso Labate, G. Ciardelli, (2017) Non-covalently crosslinked chitosan nanofibrous mats prepared by electrospinning as substrates for soft tissue regeneration. Carbohydr Polym 162:82–92. https://doi.org/10.1016/j.carbpol.2017.01.050

[41] Bonino CA, Krebs MD, Saquing CD, Jeong SI, Shearer KL, Alsberg E, Khan SA (2011) Electrospinning alginate-based nanofibers: from blends to crosslinked low molecular weight alginate-only systems. Carbohydr Polym 85:111–119. https://doi.org/10.1016/j.carbpol.2011.02.002

[42] Gutierrez-Gonzalez J, Garcia-Cela E, Magan N, Rahatekar SS (2020) Electrospinning alginate/polyethylene oxide and curcumin composite nanofibers. Mater Lett 270:127662. https://doi.org/10.1016/j.matlet.2020.127662

[43] Gao J, Guo H, Zhao L, Zhao X, Wang L (2017) Water-stability and biological behavior of electrospun collagen/PEO fibers by environmental friendly crosslinking. Fibers Polym 18:1496–1503. https://doi.org/10.1007/s12221-017-7319-0

[44] Ji Y, Ghosh K, Shu XZ, Li B, Sokolov JC, Prestwich GD, Clark RAF, Rafailovich MH (2006) Electrospun three-dimensional hyaluronic acid nanofibrous scaffolds. Biomaterials 27:3782–3792. https://doi.org/10.1016/j.biomaterials.2006.02.037

[45] Liu Y, Yu X, Li J, Fan J, Wang M, Lei T-D, Liu J, Huang D (2015) Fabrication and properties of high-content keratin/poly (ethylene oxide) blend nanofibers using two-step crosslinking process. J Nanomater. https://doi.org/10.1155/2015/803937

[46] Doytcheva M, Stamenova R, Zvetkov V, Tsvetanov CB (1998) U.V. irradiation-induced crosslinking of solid poly(-ethylene oxide) modified with tetraalkyl ammonium salt. Polymer (Guildf) 39:6715–6721. https://doi.org/10.1016/S0032-3861(98)00133-5

[47] Kalakkunnath S, Kalika DS, Lin H, Raharjo RD, Freeman BD (2007) Molecular relaxation in cross-linked poly(-ethylene glycol) and poly(propylene glycol) diacrylate networks by dielectric spectroscopy. Polymer (Guildf) 48:579–589. https://doi.org/10.1016/j.polymer.2006.11.046

[48] Zhou C, Wang Q, Wu Q (2012) UV-initiated crosslinking of electrospun poly(ethylene oxide) nanofibers with pentaerythritol triacrylate: effect of irradiation time and incorporated cellulose nanocrystals. Carbohydr Polym 87:1779–1786. https://doi.org/10.1016/j.carbpol.2011.09.095

[49] Şimşek M, Çakmak S, Gümüşderelioğlu M (2016) Insoluble poly (ethylene oxide) nanofibrous coating materials: effects of crosslinking conditions on the matrix stability. J Polym Res 23:236. https://doi.org/10.1007/s10965-016-1127-x

[50] Şimşek M, Aldemir SD, Gümüşderelioğlu M (2019) Anti-cellular PEO coatings on titanium surfaces by sequential electrospinning and crosslinking processes. Emergent Mater 2:169–179. https://doi.org/10.1007/s42247-019-00040-w

[51] McAvoy K, Jones D, Thakur RRS (2018) Synthesis and characterisation of photocrosslinked poly(ethylene glycol) diacrylate implants for sustained ocular drug delivery. Pharm Res. https://doi.org/10.1007/s11095-017-2298-9

[52] Üzüm ÖB, Karadağ E (2007) Swelling characterization of poly (acrylamide-co-N-vinylimidazole) hydrogels cross-linked by TMPTA and semi-IPN's with PEG. J Polym Res 14:483–488. https://doi.org/10.1007/s10965-007-9132-8

[53] Karadağ E, Saraydin D (2002) Swelling studies of super water retainer acrylamide/crotonic acid hydrogels cross-linked by trimethylolpropane triacrylate and 1,4-butanediol dimethacrylate. Polym Bull 48:299–307. https://doi.org/10.1007/s00289-002-0029-8

[54] Andrzejewska E (2001) Photopolymerization kinetics of multifunctional monomers. Prog Polym Sci 26:605–665. https://doi.org/10.1016/S0079-6700(01)00004-1

[55] Yoshihara T, Tadokoro H, Murahashi S (1964) Normal vibrations of the polymer molecules of helical conformation. IV. polyethylene oxide and polyethylene-d4 oxide. J Chem Phys 41:2902–2911. https://doi.org/10.1063/1.1726373

[56] Pucić I, Jurkin T (2012) FTIR assessment of poly(ethylene oxide) irradiated in solid state, melt and aqueous solution. Radiat Phys Chem 81:1426–1429. https://doi.org/10.1016/j.radphyschem.2011.12.005

[57] Zardalidis G, Mars J, Allgaier J, Mezger M, Richter D, Floudas G (2016) Influence of chain topology on polymer crystallization: poly (ethylene oxide)(PEO) rings vs. linear

chains. Soft Matter 12:8124–8134. https://doi.org/10.1039/C6SM01622G

[58] ASTM E96/E96M-16 (2016) Standard test methods for water vapor transmission of materials. ASTM International, West Conshohocken, PA. www.astm.org, https://doi.org/10.1520/E0096_E0096M-16

Publisher's Note Springer Nature remains neutral with regard to jurisdictional claims in published maps and institutional affiliations.